JOURNAL OF MATERIALS SCIENCE **36** (2001) 739–750

Solidification and precipitation behaviour of Al-Si-Mg casting alloys

Q. G. WANG*
Department of Mining, Minerals and Materials Engineering, The University of Queensland, Brisbane, QLD 4072, Australia

C. J. DAVIDSON
CSIRO Manufacturing Science and Technology, PO Box 883, Kenmore, Australia
E-mail: Cameron.Davidson@cmst.csiro.au

The effect of Mg content on the solidification and precipitation behaviour of both unmodified and Sr-modified Al-7Si-Mg casting alloys has been investigated at various solidification rates using cooling curve analysis, differential scanning calorimetry (DSC) and optical and electron microscopy. The Mg concentrations covered the range from 0.3 wt% to 0.7 wt%. The results indicate that increasing Mg content or cooling rate lowers the liquidus and binary Al-Si eutectic transformation temperatures. The latent heat of fusion of these alloys is strongly dependent on the level of Si present, but there is no observed dependence on Mg content. The solidification reactions observed under DSC are identified and it is noticed that the ternary eutectic solidification reaction $L \rightarrow Al + Si + Mg_2Si$ is only observed at Mg levels of 0.6% and higher. The minor phases formed on solidification are identified and their response to solution heat treatment is examined. Increasing Mg content usually enhances precipitate hardening. However when Mg levels are increased above 0.5wt%, no apparent increase of yield strength with Mg is observed. This is correlated with dissolved Mg levels and energy released during reprecipitation.

1. Introduction

Al-Si-Mg casting alloys are being increasingly used in automotive and aerospace industries for critical structure applications because of their excellent castability and corrosion resistance and, in particular, good mechanical properties in the heat-treated condition.

In these casting alloys, Mg is intentionally added to induce age hardening through Mg-Si precipitation [1, 2, 3]. However, the increased Mg content decreases the ductility and fracture toughness of the materials [4, 5]. This suggests that, while Mg achieves the aim of making the aluminium matrix age-hardenable, it might also influence the microstructure and particularly the type and morphology of brittle phases. This has been substantiated by some excellent work published in the literature. Bäckerud *et al*. [6] studied three types of Al-Si-Mg casting alloys (A356.1, A356.2, and A357.2) and discussed the solidification characteristics of these alloys under three cooling rates. It was observed that the addition of Mg changed the solidification sequence and the type of Fe-bearing intermetallics. However, it is difficult to conclude the actual effect of Mg because their higher Mg alloy (0.56%Mg) contained a small amount of beryllium, which is known to strongly influence the behaviour of Fe. Granger *et al*. [7] in their study found that beryllium-free alloy (A357.0) had an insoluble Fe-bearing phase containing Mg, while the alloy with beryllium (A357.2) did not. Tan *et al*. [8] obtained similar results. Joenoes and Gruzleski [9] studied the effect of Mg content in iron-free synthetic alloys at a constant cooling rate. They found that a small amount of Mg changed the morphology and size distributions of the silicon phase. In the modified alloy, Mg also combined with Sr to form a complex $Mg_2SrAl_4Si_3$ intermetallic compound which was thought probably to have been formed prior to the eutectic transformation.

Although the influence of Mg on the eutectic Si particles has been recognized in the literature, there is a dearth of information pertaining to the optimization of Mg addition. The mechanisms by which Mg influences the formation and distribution of the minor phases (in particular the Fe-bearing intermetallic phases) are still not well understood. In one recent work that addressed this issue, Mackay and Gruzleski [10] studied the interrelation between Fe and Mg levels on cooling curve characteristics in an unmodified Al-7.2%Si alloy. They reported that at Mg levels below 0.5 wt%, the only solidification reaction involving Mg-based phases that was discernible on the cooling curves was the ternary eutectic forming Al, Si and Mg_2Si, starting at approximately 555°C. At Mg levels above 0.5% (unless Fe was very high) a separate reaction was observed

* *Present Address:* Advanced Materials Development Center, General Motors–Powertrain, Saginaw, Michigan, 48605 USA; e-mail: Qigui. Wang@gm. com

starting 10°C higher in the cooling curves and forming $Al_8Mg_3FeSi_6$ in addition to the above three phases. Even more recently, Taylor *et al*. [11] have examined in detail the influence of Mg on solution heat-treatment of the cast alloys and they have reported relative volume fractions of each of the minor phases. In the as-cast state the π-phase was found at levels of around 1% by volume, independent of Mg level, while β-phase and Mg_2Si were each generally less than 0.1 vol%, with Mg_2Si rising to about 0.2 vol% at 0.7 wt% Mg. Solution heat-treatment reduced the amount of Mg_2Si at all compositions but substantially reduced the amount of π-phase only in the alloys where Mg levels were 0.3 or 0.4 wt%.

This work is aimed at evaluating the effect of Mg content on the solidification and precipitation behaviour of commercial Al-Si-Mg castings solidified at different cooling rates, and at providing a basis for optimizing the Mg content of these alloys.

2. Experimental procedure

2.1. Materials

Commercial unmodified Al-7%Si-0.3 ~ 0.7%Mg casting alloys (alloys 601 and 603, Australian nomenclature, similar to the US A356.0 and A357.0) were used in this investigation. Modification was achieved by adding an Al-10%Sr master alloy to the unmodified melt just prior to degassing. The chemical compositions of the alloys are shown in Table I. Throughout this work, alloys are suffixed by "um" for unmodified and "Sr" for strontium-modified. Samples with a range of secondary dendrite arm spacing were produced by an end-chill sand casting procedure, details of which have been described elsewhere [12, 13].

A laboratory-prepared Al-7%Si binary alloy and a commercial Al-12%Si alloy were also used for reference in DSC measurements.

2.2. Thermal analysis

Conventional cooling curve measurements were carried out on samples of the Sr-modified 601 and 603 alloys that were cast in cylindrical sand and metal moulds of 50 mm diameter. The cooling curves were obtained by placing two K-type thermocouples at the center and wall of the mould and recording the temperature change as a function of time during solidification using a data acquisition system. The thermocouples were fixed at the same distance (25 mm) from the bottom of the moulds for all runs. The pouring temperatures were kept around 745°C for all experiments.

Differential scanning calorimetry (DSC) analysis was performed on samples of all studied alloys using a PERKIN-ELMER DSC-7 instrument. Specimens used were discs, ~4 mm in diameter and weighing from 10 to 25 mg, depending on temperature, scanning rate, and the type of test being carried out.

Latent heat measurements were carried out over a range of cooling rates, from 2 to 60°C/min. Temperatures were calibrated against pure In and Al and the energy was calibrated using 397 kJ/kg for the latent heat of fusion of Al. The energy calibration agreed well with that of In, indicating good linearity across the temperature range of the equipment. Repeated calibrations showed the equipment remained within ±1% during the tests. During latent heat measurements the reference pan was left empty, and a scan of the sample pan with no sample was used as the baseline reference.

In the study of phase transformation during solidification or remelting, the DSC was run at a scanning rate of 10°C/min over the range of 500°C to 650°C. A high-purity aluminium disc of similar weight to the samples was used in the reference pan. For precipitation characterization, DSC thermograms from 50°C to 500°C were acquired using a heating rate of 30°C/min on T4 heat-treated samples. This heat treatment consisted of solution treatment at 540°C for 20 h followed by quenching into water at room-temperature. Quenched samples were either transferred directly to the DSC equipment, or, if this was not possible, then they were immediately placed in a freeezer at a temperature of approximately −10°C. The total time at room temperature between quenching and DSC measurement did not exceed 10 minutes. The total time in the freezer for any sample did not exceed 30 minutes.

In interpreting the temperatures reported by the DSC equipment it is important to consider its design. The sample sits in a pan which sits on a heating element. A Pt resistance thermometer is integrated into the heating element and this is the temperature recorded by the equipment. A second similar heater and pan provides the reference and the recorded power is the difference between the two systems. There is no direct measurement of the sample temperature such as there is in simple cooling curves. There is always a temperature lag between the sample and the temperature sensor and this lag increases with increasing values of heat flux and the

TABLE I Chemical compositions (wt percent) of the alloys

Alloys	Si	Mg	Sr	Fe	Ti	Cr, Cu, Mn, Ni, Zn, Zr
601Sr (0.3Mg)	7.0	0.3	0.019	0.13	0.13	<0.01, each
601um (0.4Mg)	6.8	0.39	<0.001	0.13	0.13	<0.01, each
601Sr (0.4Mg)	7.0	0.41	0.019	0.14	0.13	<0.01, each
603um (0.5Mg)	7.2	0.51	<0.001	0.15	0.11	<0.01, each
603um (0.6Mg)	6.9	0.60	<0.001	0.14	0.09	<0.01, each
603Sr (0.6Mg)	6.8	0.58	0.020	0.14	0.09	<0.01, each
603Sr (0.7Mg)	6.9	0.7	0.020	0.13	0.10	<0.01, each
Al-7Si	7.3	<0.01	<0.001	0.09	<0.005	not recorded
Al-12Si	12.3	<0.05	<0.001	0.15	n/r	not recorded

thermal resistance between sample and sensor. Under normal operation this is calibrated out quite precisely, so long as the heating rate is not changed, but when the heat flux increases significantly from the calibration state then the temperature lag increases significantly. Thus, during solidification, when heat fluxes are several W/g from the baseline, temperature deviations of the order of several degrees are to be expected. Furthermore, there will even be a temperature gradient across the sample itself, which will appear to smear out the temperature range of a reaction. This effect becomes greater with any increase in the rate at which energy is released or absorbed. Correcting for these effects is difficult to do accurately and has not been attempted for the results presented here. Temperature onsets and ranges reported here should be interpreted with regard to these considerations.

2.3. Microscopic analysis

All samples for metallographic examination were prepared using standard techniques. Following a 1 μm diamond finish, the final polish was achieved using commercial SiO_2 slurry (Struers OP-U).

Chemical constitution and compositions of the aluminum matrix and Fe-bearing intermetallic phases were measured on polished samples. Energy-dispersive X-ray Spectrometry (EDX) in a JEOL 6400F scanning electron microscope was used for qualitative analysis and a JEOL JXA-8800 electron probe microanalyzer (EPMA) with wavelength-dispersive spectrometers was used for quantitative microanalysis. Freshly polished pure metals were used as standards.

3. Results

3.1. Cooling curves

The cooling curves of alloys 601 and 603 with different Mg contents and cooling rates during solidification are shown in Fig. 1 together with their differentiated curves. For comparative purposes in this study, the cooling rate is defined as shown in Fig. 1, by dT/dt computed from the approximately straight line portion during the later stages of primary dendrite growth. It can be seen that the solidification sequence of alloys 601/603 consists mainly of three phase transformations: firstly, the formation of aluminium dendrites corresponding to the first peak in the derivative of the cooling curves; secondly, the main binary eutectic reaction, represented by the second peak; and thirdly, the formation of ternary and/or quaternary eutectic phases such as Mg_2Si and/or Fe-bearing intermetallics, which are difficult to observe from the cooling curves, particularly in the case of the higher cooling rate. From the results of the cooling curve analyses, the effects of Mg content and cooling rate during solidification on the liquidus and binary eutectic temperature are illustrated in Fig. 2. It is seen that increasing the Mg content and cooling rate shifts the liquidus and binary eutectic transformations to a lower temperature. It should be stated here that we are not referring to the invariant pure binary Al-Si eutectic reaction, but to the start of the temperature range over which Al-rich and Si-rich phases solidify together from the liquid in a microstructure similar to the Al-Si eutectic. The minor elements will, of course, provide some extra degrees of freedom to this phase transformation and the solid that forms will be poorer in Mg and Fe than the remaining liquid.

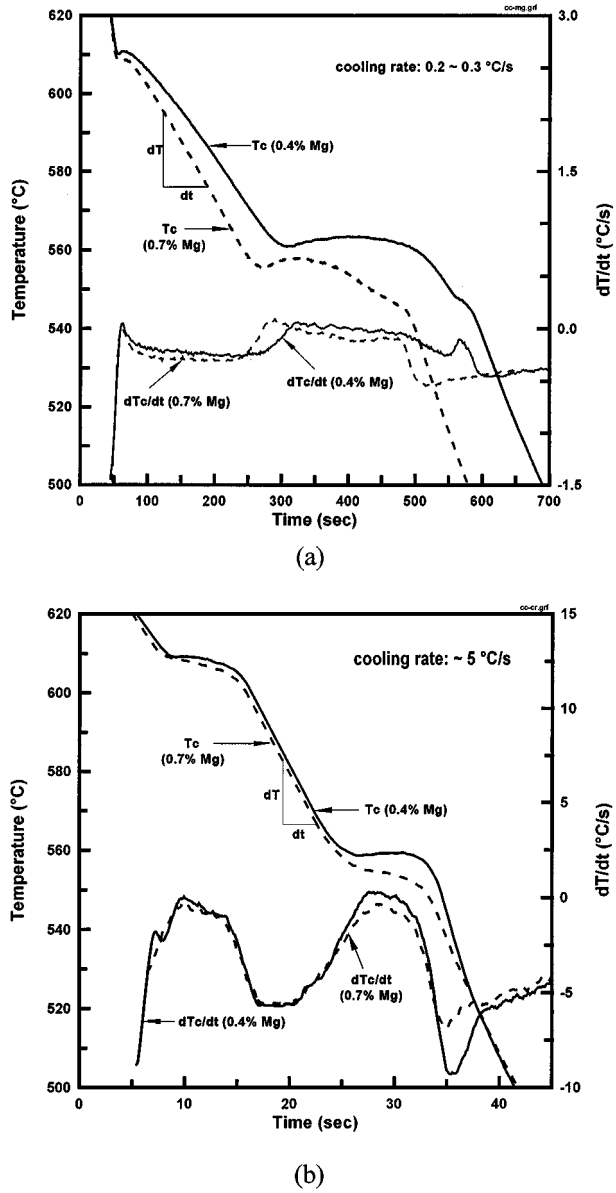

Figure 1 Cooling curves obtained from two Sr-modified alloys with moderate and high Mg levels at different cooling rates: (a) 0.2–0.3°C/s and (b) ~5°C/s.

3.2. Microstructure

As-cast microstructures showed the expected minor phases (π–AlFeMgSi, β-AlFeSi and Mg_2Si), in varying amounts depending on the bulk Mg level. The π–phase was the dominant phase in the as-cast condition throughout the range of compositions, but the proportion of Mg_2Si increased as the Mg levels increased.

Fig. 3 shows backscattered-electron SEM images from slowly solidified high-Mg 603 alloy, in which it can be readily seen that the π-phase often grows in close association with β-phase particles.

Fig. 4 compares the microstructures of the low and high Mg alloys after solution treatment and ageing. The Fe-bearing particles in the low Mg 601 alloys were apparently mainly β-phase (Al_5FeSi), but they

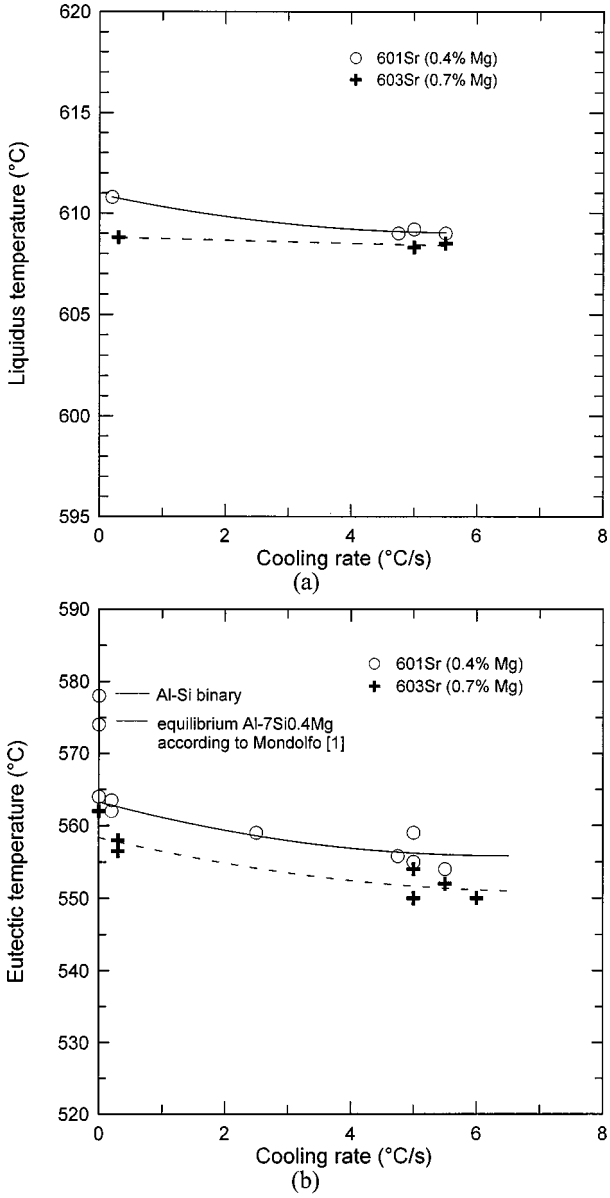

Figure 2 The solidification temperatures of (a) the liquidus and (b) the binary eutectic as a function of cooling rate in alloys with two levels of Mg. Values were determined from cooling curve analysis.

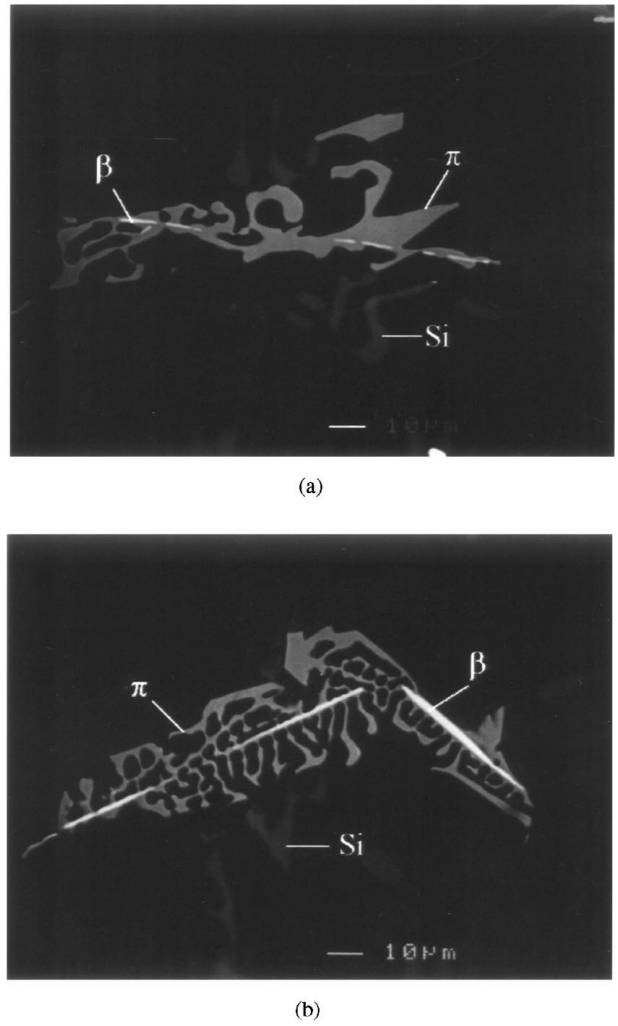

Figure 3 SEM backscattered-electron images of as-cast 603-Sr alloy showing the close association sometimes observed between π-AlFeMgSi and β-AlFeSi.

were present in two fairly distinct forms: the as-cast plates (exhibiting a small degree of spheroidisation); and clusters of very fine plates, which are too small to be visible in Fig. 4 and too small for accurate microprobe analysis. There was also a small spheroidised globular phase, probably π-AlFeMgSi, in close association with the fine plates. In the high Mg 603 alloys the Fe-bearing particles were mainly π-AlFeMgSi. The number and size of Fe-bearing intermetallics increased with increasing Mg. Quantitative details of particle size and fraction of Fe-bearing phase particles after T6 heat treatment have been reported elsewhere [5, 14].

The EPMA analyses of the π-phase in both the as-cast and the T6 condition gave formulae close to $Al_9FeMg_3Si_5$, rather than the stoichiometric $Al_8FeMg_3Si_6$. This agrees with the findings of Simensen and Rolfsen [15] and Tan *et al*. [8], who concluded that Al and, to some extent, Mg could replace Si in the crystal lattice of the π-phase.

Table II compares the Mg and Fe concentrations in the aluminium matrix before and after T4 solution

TABLE II The Mg and Fe concentrations in the aluminum matrix before and after solution treatment, as determined by Xray microanalysis. All measurements were on areas of the casting where DAS was 30 to 35 μm. Sample standard deviations based on 20 measurements are listed in parentheses

Alloy	As-cast		After solution treatment	
Mg (wt %)	Mg (wt %)	Fe (wt %)	Mg (wt %)	Fe (wt %)
0.3 (601Sr)	0.151	0.009 (0.007)	0.293 (0.027)	0.010 (0.006)
0.4 (601Sr)	0.199	0.009 (0.006)	0.389 (0.020)	0.009 (0.005)
0.5 (603Sr)	0.231	0.007 (0.004)	0.489 (0.026)	0.005 (0.002)
0.6 (603Sr)	0.263	0.007 (0.003)	0.489 (0.020)	0.006 (0.002)
0.7 (603Sr)	0.287	0.006 (0.004)	0.509 (0.037)	0.007 (0.005)

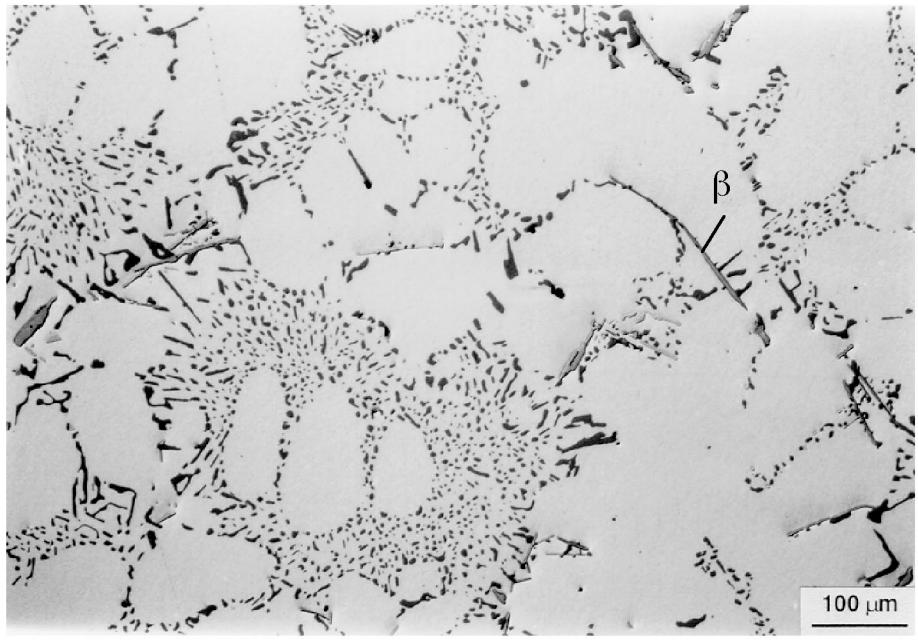

(a)

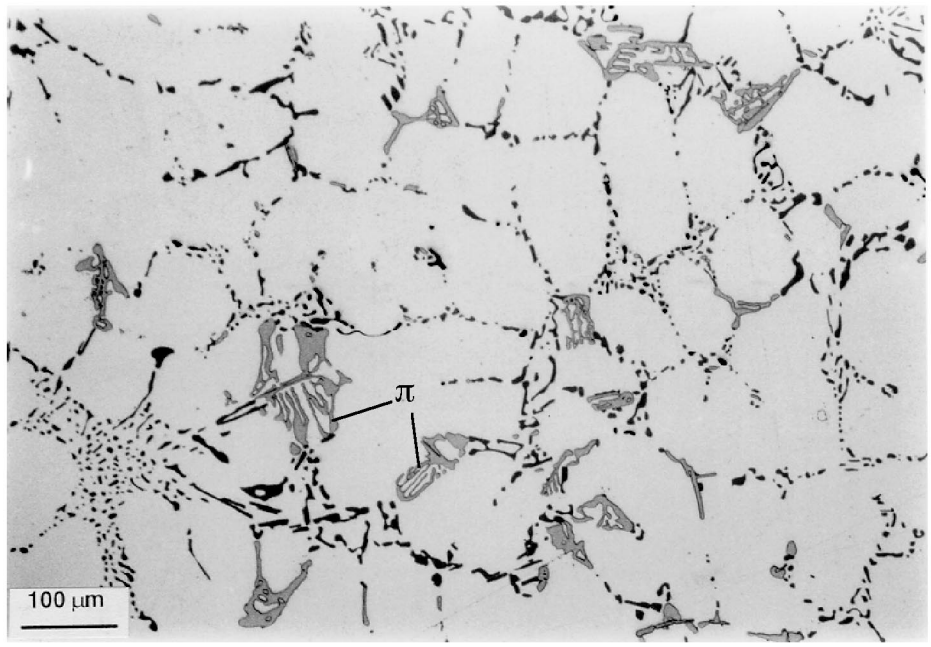

(b)

Figure 4 Typical microstructures of (a) 601Sr-T6 (0.4% Mg) and (b) 603Sr-T6 (0.7% Mg) solidified at a cooling rate of 0.2 °C/s.

treatment. These values for Mg are plotted in Fig. 5 as a function of the Mg concentration in the bulk alloy. The Mg levels in the as-cast matrix are only average values for the purpose of indicating the trend, since they do not show the microsegregation. As expected, solution treatment resulted in an increase in the amount of Mg in the solid solution. In the 603 alloy containing 0.5% Mg, the amount of Mg found in the matrix after solution treatment is around 0.49%. Increasing the Mg level in the bulk alloy beyond 0.5% results in only slight increase in the amount of Mg in the matrix after solution treatment – it remains at around 0.5%. The Fe content in the matrix is very low and does not change with heat-treatment. In fact, the values are close to the detection limits under the conditions used, and the minor variations are probably not significant.

Fig. 6 shows an EPMA scan of Mg levels across two dendrite arms taken from a 0.4% Mg alloy after 1 hour solution treatment. The scan intersected a π-phase particle in the middle. The Mg level drops to 0.37 wt% at distance of 50 μm to one side of the centre, but remains at about 0.41 wt% on the other side. Examination of the microstructure showed other small π-phase particles close to the Si particle at position -60 μm, while there were none visible on the plane of section near the end of the scan at position $+60$ μm.

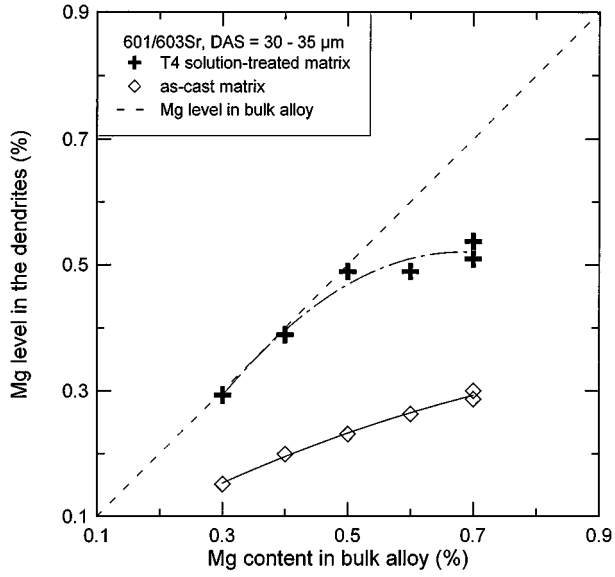

Figure 5 The Mg content in the as-cast and the T4 solution-treated matrix of various Al-Si-Mg casting alloys.

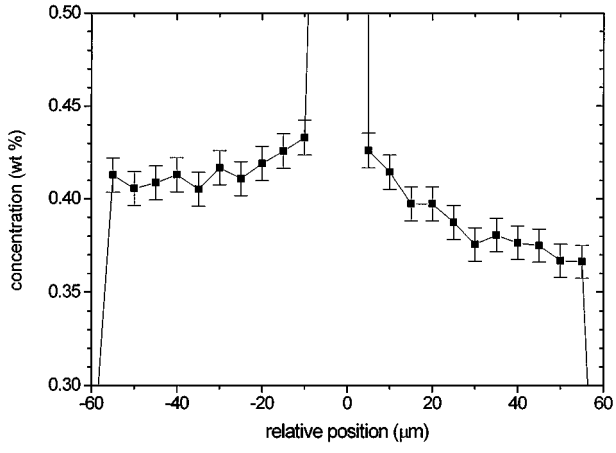

Figure 6 Mg concentration profile across two dendrite arms in 601-um (0.4%Mg) after 1 hour solution treatment at 540°C. The scan intersected interdendritic Si particles at -60 and $+60$ μm and a π-phase particle at position zero. Error bars show three standard deviations derived from Poisson counting statistics.

3.3. DSC thermograms

3.3.1. Solidification characteristics

Fig. 7 shows a typical DSC trace for melting and solidification of an as-cast 603Sr sample scanned at a heating/cooling rate of 10 °C/min. In the DSC curves the reaction peaks reflect the specific phase changes and the peak area is proportional to the heat of reaction (ΔH_R) associated with the phase transformation. Positive values of ΔH_R are due to the endothermic reactions of liquid formation during heating, while negative values result from the latent heat released during solidification. As shown in Fig. 7, there are four reaction peaks for this high Mg alloy in both heating and cooling curves. Peak 1 corresponds to the development of aluminium dendrites; peak 2 represents the main binary eutectic reaction; peaks 3a and 3b are associated with formation of the minor phases and will be discussed below.

The influence of increasing Mg content from 0.3% to 0.7% on the solidification behaviour of various Al-

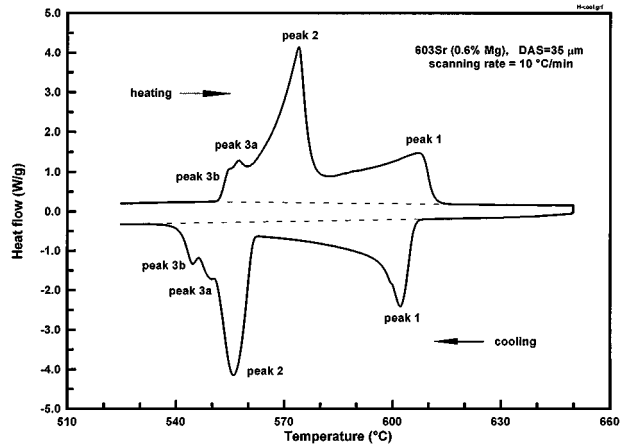

Figure 7 Typical DSC curves for an as-cast 603Sr sample run at a scanning rate of 10°C/min.

Si-Mg casting alloys is illustrated by the DSC plots in Fig. 8. The most immediately apparent feature is that, while peaks 3a and 3b are evident in the high-Mg alloys, only one part of peak 3 is visible at Mg levels 0.4% or lower. There is some ambiguity in the cooling DSC curves as to which peak is present at low Mg, but it seems quite clear from the heating curves that peak 3b is present at all Mg levels, while peak 3a is only present at high Mg. Tables III and IV tabulate the characteristics of the DSC curves in Fig. 8. The reported values of ΔH_R are derived using a local baseline, however

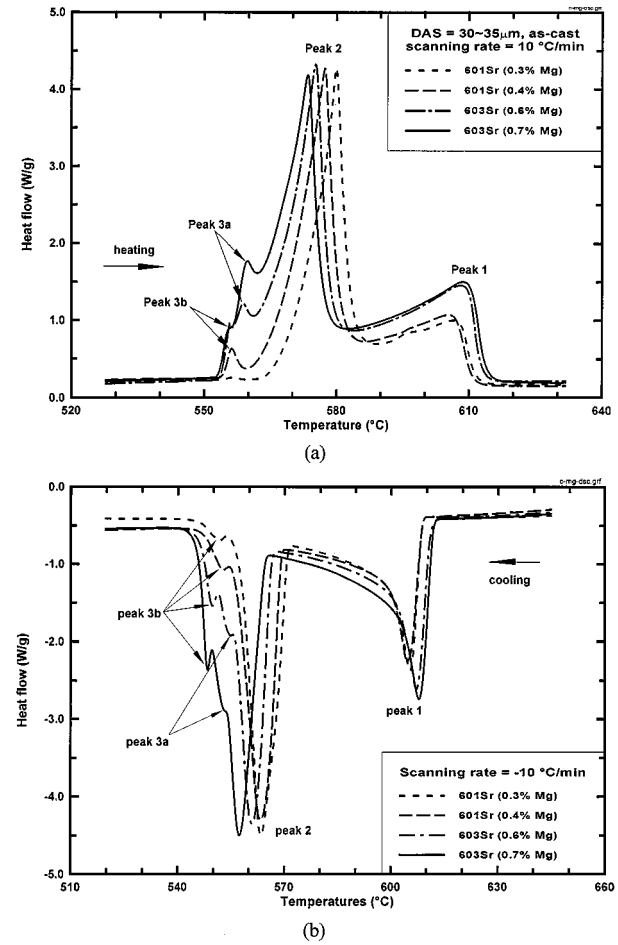

Figure 8 DSC curves, showing the effect of Mg addition on the melting/solidification behaviour in (a) heating and (b) cooling.

TABLE III DSC remelting characteristics of the as-cast 601Sr and 603Sr alloys. The data listed in parentheses are standard deviations based on 5 measurements

	Mg_2Si and Fe-bearing phase reactions (peaks 3a and b)			Binary eutectic (peak 2)
Alloys	Temp. range (° C)	Onset (° C)	ΔH_R (J/g)	Temp. range (° C)
601Sr (0.3% Mg)	553–559	554.8 (2.1)	0.37 (0.17)	561–588
601Sr (0.4% Mg)	554–559	554.4 (2.3)	5.49 (1.27)	559–585
603Sr (0.6% Mg)	554–562	554.9 (3.0)	17.3 (2.64)	562–583
603Sr (0.7% Mg)	554–564	554.4 (2.0)	22.63 (1.43)	564–579

there is substantial overlap with the adjacent peaks, especially from peak 2 but also between 3a and 3b, and so the values are likely to underestimate the true heats of reaction for the minor peaks. From the DSC curves and their characteristics, it is seen that a small amount of Mg addition has a marked effect on the solidification behaviour. Increasing Mg content decreases the binary eutectic temperatures as observed in both heating and cooling DSC curves, which is in good agreement with our cooling curve analyses and the findings published in the literature [9, 16, 17]. The positions of peaks for the minor phase reactions show a slight decrease of temperatures with increasing Mg in the cooling DSC curves. However, as explained above, the temperature in this DSC equipment cannot be considered well calibrated in the presence of adjacent major peaks. With increasing Mg the minor peaks occur with more overlap from peak 2 and it is therefore quite possible that increasing temperature offset would occur, canceling or even reversing the apparent shift with Mg. Therefore no reliable conclusion can be drawn from this evidence. When heated from the as-cast state, Fig. 8a, the onset of melting seems to be independent of Mg content and peaks 3a and 3b are so heavily overlapped that it is not possible to determine separate values.

3.3.2. Latent heat of fusion

The latent heat of the near-eutectic Al-12.3%Si was determined to be about 495 kJ/kg. The latent heat values for some 7 wt% Si alloys are plotted in Fig. 9 as a function of cooling rate. There is no apparent dependence on Mg content or on the presence of Sr. On the other hand, there is, at first sight, a variation with cooling rate, with

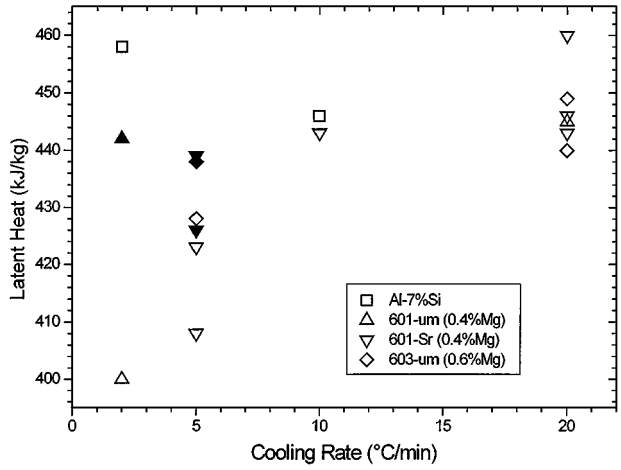

Figure 9 Latent heat released during solidification for various alloys as a function of cooling rate. The hollow symbols are derived from a linear baseline, while the solid symbols are recalculations after fitting curved baselines.

lower cooling rates giving lower latent heat values. This is attributed to baseline curvature, to which these hypoeutectic alloys are quite sensitive because they have freezing ranges of 40 to 70 °C. The software supplied with the DSC equipment only allows use of a linear baseline and the values that were below 440 kJ/kg were seen to come from curves that had a baseline that apparently curved up in the middle. DSC traces giving results over 440 kJ/kg had baselines that appeared to be linear. A subjectively-drawn, curved baseline was applied to the relevant curves and the recalculated areas are plotted in Fig. 9 as solid symbols. They show substantially better agreement with the results from samples with linear baselines.

The fraction of energy released by the primary phase solidification was determined by separately measuring the area under the curve from liquidus to the point of zero slope where the Al-Si eutectic begins. The mean value of this was 0.43. The value showed a slight variation with alloy composition, but that correlated well with the small variations in Si content. Note that, although increasing Mg leads to broadening of the tail of peak 2 and to the extra minor peaks, the area under the combined peaks 2 and 3 was independent of Mg level.

If we assume that the latent heat from peaks 2 and 3 is equal to the value measured for the Al-Si eutectic and that the latent heat for the primary phase is equal to that for pure Al then, without assuming any value for the latent heat of the 7%Si alloys, we can calculate that the mass fraction of primary phase is 0.48 ± 0.02. This

TABLE IV DSC solidification characteristics of the 601Sr and 603Sr alloys. Sample standard deviations from 5 measurements are listed in parentheses

	Peak 3b			Peak 3a			Binary eutectic (peak 2)	
Alloys	Temp. range (° C)	Onset (° C)	ΔH_R (J/g)	Temp range (° C)	Onset (° C)	ΔH_R (J/g)	Temp. range (° C)	Onset (° C)
601Sr (0.3% Mg)	547–554	553.4 (2.1)	−2.6 (0.2)	—	—	—	554–572	570.8 (1.8)
601Sr (0.4% Mg)	548–555	554.4 (1.6)	−3.7 (0.3)	—	—	—	554–570	568.9 (1.3)
603Sr (0.6% Mg)	546–552	551.2 (1.9)	−3.0 (0.1)	552–556	555.6	−1.6 (0.1)	555–567	566.1 (0.9)
603Sr (0.7% Mg)	545–550	549.5 (2.7)	−3.3 (0.2)	550–554	553.0	−2.0 (0.2)	553–566	563.7 (2.1)
603um (0.6% Mg)	547–553	552.5 (1.4)	−2.8 (0.1)	553–557	557.1	−1.4 (0.1)	557–570	568.8 (1.3)

value leads to a weighted average latent heat value of 447 ± 4 kJ/kg, if we assume a 1% error for the latent heat of the eutectic and negligible error in the primary phase latent heat value.

3.3.3. Precipitation characteristics

A selection of alloys, covering two different dendrite arm spacings, with and without Sr modification, with Mg levels from 0.3 to 0.7 wt% were given a T4 solution heat treatment and then heated in the DSC at 30°C/min to investigate the solid state precipitation reactions. The results are presented in Table V and typical curves from these tests are shown in Fig. 10. At Mg contents of 0.4 wt% and above there are three distinct peaks, designated A, B and C in increasing temperature of occurrence.

Neither the dendrite arm spacing nor the presence of Sr-modification seems to have any influence on the precipitation behaviour. The total peak area is consistently higher for the unmodified alloys, but there is enough scatter in the data that it is unlikely to be significant. There is a general trend of increasing peak area with increasing Mg content, but there is only a 20% increase with a doubling of Mg level.

The influence of Mg concentration on the reaction temperatures is illustrated in Fig. 11. The increase of

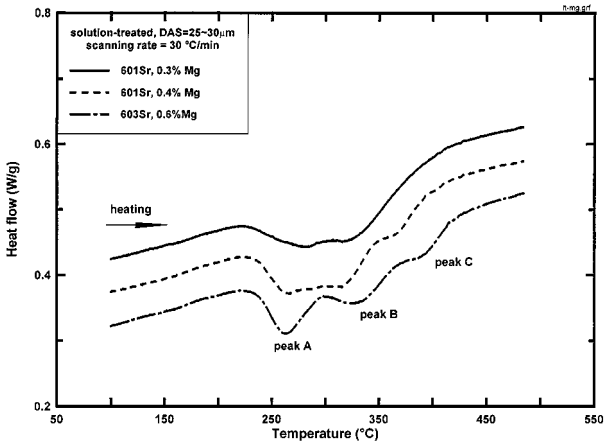

Figure 10 The DSC curves illustrating the effect of Mg content on the precipitation behaviour.

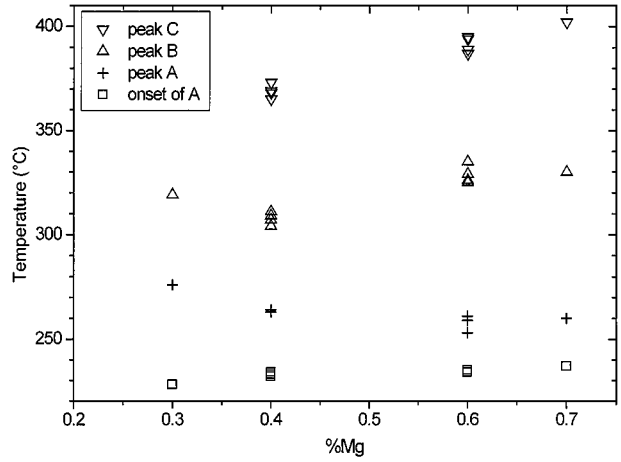

Figure 11 Effect of Mg content on peak temperatures recorded when reheating solution-treated alloys.

Mg content from 0.3 to 0.4% significantly decreases the temperature of peak A but there is only a slight further decrease in temperature for Mg levels above 0.4%. On the other hand, the onset temperature for peak A shows a very slight increase with increasing Mg. Likewise, peaks B and C increase temperature with increasing Mg, except for 0.3% Mg. This suggests that at 0.3% Mg the peaks B and C may have overlapped enough to appear as a single peak, with a temperature part way between expected values for two separate peaks.

4. Discussion

4.1. Effect of Mg on solidification temperatures

The cooling curve and DSC thermal analysis showed that, during solidification, increasing Mg content from 0.4 to 0.7 wt% suppressed the liquidus by 1–2°C and the start of the Al-Si binary eutectic reaction by 5°C. According to an empirical formula attributed [16] to Mondolfo [1], the basic unmodified binary eutectic temperature for Al-7Si-0.13Fe will decrease by 2.4°C as Mg increases by 0.3 wt%. The results of Joenoes and Gruzleski [9] suggest a drop of 5°C over that range of Mg, while those of Mackay and Gruzleski [10], at a much slower cooling rate, suggest between 2.5 and 3°C. If we consider the Al-Si-Mg ternary system, the

TABLE V DSC precipitation characteristics of solution-treated 601 and 603 alloys during reheating at 30°C/min. Standard deviations are listed in parentheses

Alloys			peak A		peak B	peak C	whole precipitation	
DAS (μm)	Mg (wt%)	mod.	Onset (° C)	T_p (° C)	T_p (° C)	T_p (° C)	Temp. range (°C)	ΔH_R (J/g)
17	0.4	Sr	233 (3.0)	264 (3.6)	311 (4.5)	368 (2.8)	216–411	−27.1 (2.2)
25–30	0.3	Sr	228 (2.1)	276 (1.7)	319 (3.6)	—	213–412	−25.1 (1.7)
	0.4	Sr	234 (4.0)	263 (4.1)	309 (4.4)	373 (3.7)	218–423	−28.2 (2.2)
	0.4	none	232 (3.5)	263 (3.8)	307 (3.2)	365 (3.6)	216–416	−28.6 (2.0)
	0.6	Sr	234 (3.7)	261 (4.7)	325 (2.8)	389 (4.3)	220–421	−28.9 (2.3)
	0.6	none	235 (3.1)	259 (3.4)	326 (4.7)	387 (3.1)	220–431	−29.2 (3.1)
	0.7	Sr	237 (2.7)	260 (3.6)	330 (3.1)	402 (4.5)	222–454	−29.6 (3.5)
50–55	0.4	Sr	233 (1.7)	264 (1.1)	307 (4.0)	369 (2.8)	220–400	−26.0 (1.4)
	0.4	none	232 (3.6)	263 (2.4)	304 (4.1)	368 (3.1)	214–408	−28.9 (1.1)
	0.6	Sr	234 (2.4)	261 (3.2)	329 (2.7)	395 (2.9)	221–430	−28.4 (2.7)
	0.6	none	234 (3.4)	253 (3.7)	335 (2.9)	394 (3.3)	217–431	−29.1 (3.5)

liquidus in the eutectic trough between the Al-Si eutectic and the ternary eutectic drops by 23°C over 5%Mg. Thus, if the liquidus is linear with Mg then the equilibrium effect of changing Mg from 0.4 to 0.7 wt% should be 1.4°C. Either the liquidus is quite concave or there may be some other effect. Since Mg has a slight modifying effect on the Si morphology [9] it may be that there is an added undercooling associated with this, as there is with Sr and Na. Very careful reheating measurements would be required to validate this, but the DSC is not a suitable apparatus to do this and the results presented here can neither confirm nor deny the hypothesis.

It has generally been reported that Sr-modification depresses the binary eutectic temperature 8 to 10°C [6, 18, 19]. In the cooling curves (Fig. 2b), there is indeed a depression of 10°C from the expected temperature at low cooling rates. However, in the DSC, Sr-modified alloys showed a reduction of only 1–2 °C compared to the unmodified state. There are very few reports in the literature of such minimal depressions - Joenoes and Gruzleski [9] found that the depression decreased from 5°C with zero Mg content to less that 1°C with 1 wt%Mg. However if their results up to only 0.7%Mg are considered then a trend of 5°C depression, independent of Mg level, is found. A sample of the Sr-modified alloy that had been used in the DSC solidification experiments was examined metallographically and it was found that that sample had a microstructure that was almost completely unmodified. This suggested that the very low values observed by DSC in this study were the result of premature fading of the Sr, due to the very thin sample sizes.

4.2. Solidification sequence

The typical solidification sequence noted in the literature for Al-7Si-Mg alloys is presented in Table VI [6]. Note that we have not changed the *reaction* numbering of Bäckerud *et al*., so it is not necessarily the same as our *peak* numbering. In this discussion we distinguish between them by always using the name *reaction* or *peak*. In step 1, the primary aluminium dendritic phase nucleates and grows. In stage 2, the main Al-Si binary eutectic reaction (2) takes place. The Fe is partitioning strongly to the liquid phase, enriching it as the fraction of liquid decreases, until the ternary eutectic is reached, solidifying Al, Si, and β-AlFeSi. Subsequently, the β-phase is partly transformed into the π-phase through a quasi-peritectic reaction (3b) [6]. However, the extent of this peritectic transformation probably depends on the cooling rate during solidification. The last stages are the ternary eutectic producing Al, Si and Mg_2Si (reaction 4), and finally a quaternary reaction giving π-AlFeMgSi in addition to the previous 3 phases. Furthermore, α-Al(Fe, Mn)Si has been reported in the final stages in higher Mg alloy [6].

The major reactions 1 and 2 are clearly evident from the microstructure and thermal analysis. Reaction 3b is supported directly by the SEM images in Fig. 3, where the π-phase is growing from β-phase and this also implies that reaction 3a must already have occurred. Neither reaction 3a nor 3b produced any thermal signature in the cooling curves of Bäckerud *et al*. and it is likely the same would apply to the DSC traces reported here. The reasons for this could be that the Al-Si and Al-Si-β-AlFeSi reactions overlap to such an extent that they are merged in the thermal traces. The peritectic reaction involves the β-phase that has supposedly already solidified in a eutectic and is therefore likely to require solid-state diffusion. This would slow down the reaction rate such that it would not be apparent in the thermal traces among the other reactions. Reactions 4 and 5 are consistent with our final microstructure and the remaining peaks on the DSC traces. Therefore in the final column of Table VI we can tentatively match our DSC peaks to the reactions.

The only contentious identifications are likely to be what reactions are associated with peaks 3a and 3b. The cooling curve derivatives published by Mackay and Gruzleski [10] have very similar characteristics to the DSC curves shown here. There is only a single minor reaction peak for Mg levels below 0.5%, occurring between 555 and 530°C. For Mg levels above 0.5% a second peak appears at approximately 560°C. The lower temperature peak was attributed by Mackay and Gruzleski to the ternary Al-Si-Mg_2Si eutectic (presumably on the basis of the temperature), while the higher temperature peak was attributed to the Al-Si-Mg_2Si-π-phase quaternary. This is the opposite of the reactions in Table VI. The order of reaction suggested in Table VI is supported by several microstructural observations. The area of the last peak is relatively independent of Mg concentration and π-phase volume fractions are similarly independent of Mg levels [11]. The volume fraction of Mg_2Si, on the other hand, is much lower than that of π-phase at all Mg levels but increases with Mg level [11, 20]. Thus both observations are consistent with the reaction assignments in Table VI. Furthermore, the higher temperature reaction was not observed by Mackay and Gruzleski when Fe content was increased to 0.55 wt%. This would be easier to explain with the reaction order proposed here.

TABLE VI Solidification reactions observed in alloys 601/603

Reaction No. defined in [6]	Reaction	Suggested start Temperature (°C) [6].	Tentative assignment to DSC peak
1	Liq. $\rightarrow$ Al dendrites	611–615	1
2	Liq. $\rightarrow$ Al + Si	577	2
3a	Liq. $\rightarrow$ Al + Si + Al_5FeSi	575	—
3b	Liq. + Al_5FeSi $\rightarrow$ Al + Si + $Al_8FeMg_3Si_6$	567	—
4	Liq. $\rightarrow$ Al + Si + Mg_2Si	555	3a
5	Liq. $\rightarrow$ Al + Si + Mg_2Si + $Al_8FeMg_3Si_6$	550–554	3b

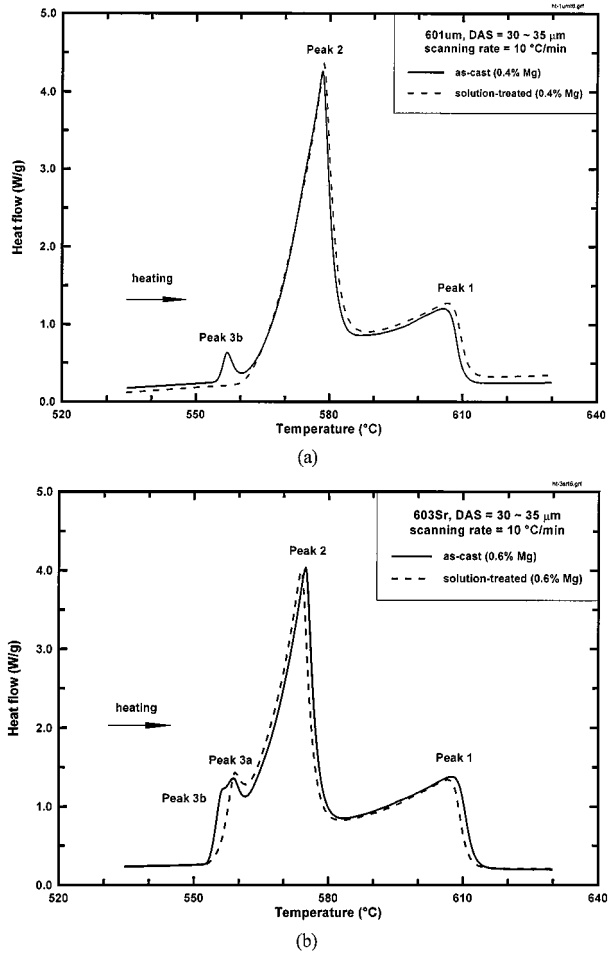

Figure 12 Comparison of DSC curves between the as-cast and the T4 solution-treated (a) 601um alloys and (b) 603Sr alloys.

On first sight, the comparison of DSC melting curves between the as-cast and the T4 solution-treated samples, Fig. 12, cannot be reconciled with the proposed solidification sequence. The behaviour of 0.4%Mg material in Fig. 12a is expected, since no Mg_2Si and very little π-phase remains after solution treatment and there is no detectable peak 3 on remelting the T4-treated sample. For the alloy with 0.6%Mg (Fig. 12b) it appears that the peak related to the quaternary eutectic (peak 3b) disappears after solution heat-treatment while peak 3a remains. This is consistent with the small amount of Mg_2Si remaining after solution treatment remelting in a ternary eutectic. However the following question must be addressed: since all four phases for the quarternary eutectic reaction are present, why is reaction 3b not observed? The answer to this probably lies in the reaction kinetics. Because the material has been solution treated, each of the phases will be spheroidised and much more widely spaced than when they formed during solidification. Creating a region that has the appropriate composition to be liquid will require solid-state diffusion from at least some of the particles, unless there happen to be points where all four phases are in contact. Points of contact are much more likely between the three phases of the ternary reaction and thus it is reasonable that this is the first melting reaction observed. Some of the growing liquid pools may then impinge upon the π-phase and promote further melting. This is probably necessary to account for the area of the peak being similar to that in the as-cast state, even though much of the Mg_2Si has been dissolved.

4.3. Latent heat

The values determined here for the latent heat of fusion are significantly higher than other published values and there is no clear reason why this should be the case. In comparing values here, we will scale everything relative to pure Al, since the same reference latent heat was not used in each case. In this study the Al-Si eutectic had a latent heat 24% above pure Al, while the Al-7Si alloys recorded an average value 12% higher. Tamminen [21] used a DSC to determine the latent heat contribution of the Si phase, and, calculating back from his reported value and interpolating to 12.3 wt% Si, probably would have measured a value around 18% above that of pure Al. Tamminen also noted that if he assumed the latent heat of Al(Si) dendrites was equal to that of pure Al then the latent heat for hypoeutectic alloys was lower than expected by a simple weighted average.

Hu and Pan [22], using a cooling curve analysis technique, reported eutectic latent heats 16% higher than pure Al, however they also reported the somewhat surprising result that 7%Si had no increase over pure Al, which was attributed to a possible reduction of 18% in the latent heat between pure Al and Al (1.7%Si) solid solution. Since such low concentrations were not examined in this study, this cannot be confirmed, however the internal consistency between our 7% and 12.3% Si results suggest that a significant reduction in latent heat at low Si is not present. Hu and Pan also concluded that 0.3% Mg and Ti/Sr additions increase latent heat, by about 5% each for an Al-7%Si alloy. An effect of Mg was not observed in this study, even at double the concentration. Likewise there was no observable variation with Sr. An effect of Ti cannot be ruled out, since Ti levels were not systematically changed in this study, but the only alloy with no added Ti (the Al-7Si binary) had a latent heat one or two percent *higher* than the average. We are unable to draw any conclusion about the influence of Sr because, as noted above, the Sr had faded due to the small sample size in the DSC.

Simensen and Rolfsen [15] examined the areas under their DTA curves and estimated the latent heat of fusion of the π-phase to be in the region of 940 kJ/kg. This value may be the subject of considerable error due to some of the primary phase solidification reaction overlapping other peaks, but it does offer some evidence that Mg levels might increase latent heat. If the total π-phase volume fraction were 1% [11] then an increase of 5 kJ/kg, or just over 1%, could be expected. This is within the experimental scatter of this study and much lower than the 5% change reported by Hu and Pan [22].

Quested *et al.* [23] have measured the latent heat of fusion of an Al-Si-Mg alloy using DSC equipment and obtained a value of 425 ± 5 kJ/kg (7% above the latent heat of pure Al). Their results do not overlap the results presented here within the stated ranges of likely error and there is no apparent reason for the disagreement. It is not clear which is more likely to be correct.

The general trend in published measurements of latent heat with varying Si content suggests that either: (a) the latent heat of hypoeutectic alloys is lower than the weighted average of Al and the Al-Si eutectic; or (b) the latent heat of Al(Si) solid solution is nearly 20% lower than that of pure Al. An alternative explanation, if the results presented here are correct, is that the other results were subject to errors in baseline determination. This would be particularly important in indirect methods such as those based on cooling curves, because energy flow is not measured directly and the rate of heat loss depends on crucible temperature. The greatest discrepancies occur at low Si contents, which have the greatest solidification temperature range, and so are most sensitive to any inaccuracy in the baseline.

4.4. Dissolution behaviour

As shown in Fig. 5, the Mg levels in the solution-treated matrix of low Mg alloys (<0.5 wt%) are almost equal to the Mg content in the bulk alloy. For bulk Mg levels over 0.5% the dissolved Mg level remains at 0.5% with the remainder of the Mg being present in the π–phase and a small amount of Mg_2Si. This suggests that this is the solubility limit of Mg in this alloy at the chosen T4 solution treatment temperature of 540°C. If the Mg content in the alloy is less than 0.5%, then it would be reasonable to assume that all the Mg would eventually be dissolved into the matrix after sufficient solution treatment and there would be little Mg-containing π-phase left in the solution-treated microstructure. This has been suggested by others [24]. The Mg_2Si is known to dissolve in the order of 15 minutes in low Mg alloys [20] but the π–phase seems to take longer. This is apparent in Fig. 6, where there is still a clear concentration gradient from the π–phase after 60 minutes. This is not surprising since both the Mg and Si from Mg_2Si can go directly into solution, however the π–phase cannot simply dissolve, because the Fe has negligible solubility in the matrix. It must therefore transform to another phase as the Mg is released, which is presumably the origin of the very fine plates of Fe-rich phase after solution treatment. These results are consistent with the more detailed study of Taylor *et al*. [11]. Rometsch *et al*. [20] suggest that homogenization is complete within 15 minutes, but this applies only to dissolution of Mg_2Si and removal of any concentration gradient from that and solidification segregation.

In the high Mg (>0.5%) alloy, the solubility restricts the maximum level of Mg in the matrix. The majority of the Mg_2Si will again dissolve rapidly (within 50 minutes) [20], with the balance of the Mg remaining in a spheroidised π-phase.

4.5. Solid-state precipitation

The solid state precipitation reactions in Al-Si-Mg casting alloys follow a similar sequence to that in wrought Al-Si-Mg alloys such as 6061, although the precise details may vary, and the DSC heating traces of the two alloy systems share many common characteristics [2, 3, 25, 26, 27]. In the temperature range 200 to 450°C there are three major precipitation reactions: β'', β' and Si [3, 25] where the first peak, with an onset of 210–220°C is the dominant component at peak strength, namely β''. There is not a total consensus as to the order of the other two reactions because the β' in 6061 (or B′ depending on Mg : Si ratio) [2, 25] and Si in binary Al-7Si [3] both show peaks around 300°C. It is beyond the scope of this work to address this issue, so they will remain peaks B and C. Garcia-Cordovilla *et al*. [25] also associated a minor peak at about 420°C with precipitation of the equilibrium phase Mg_2Si but there was no supporting TEM identification and their peak vanished if the sample was held at room temperature for 24 hours before ageing. In any case the identification of the higher temperature peaks is less important since they occur well after peak strength.

The area under the peak is usually regarded as a good indication of the amount of precipitation and hence strengthening, however in this case it is not possible to measure the area under the β'' peak due to the strong overlap with other peaks. As a first approximation, the contribution from excess Si was subtracted from the total area to give the combined $\beta'' + \beta'$ peak area. It is considered reasonable to assume that this combined area should be proportional to the area of the β'' peak alone. The excess Si in solution was calculated by assuming a total dissolved Si, dependent on Mg solute levels [11], and assigning Si to measured solute Mg in a 1 : 1 ratio. The energy of this excess solute was scaled by 15 J/g/%Si, derived from the results of Zhang, Zheng and StJohn [3]. Fig. 13 shows the plot of yield stress increment against total $Mg^{1/2}$ that was published previously [5] and on it has been overlaid a plot of the increment in peak area due to $\beta'' + \beta'$ precipitation. The graphs have the same origin but the y-axis scaling has been adjusted to match the yield stress and energy data points between 0.3 and 0.4 wt%Mg. This confirms that the previous observation, namely that yield stress increments at Mg levels above 0.5 wt% are less than might be expected, is due to a limitation on the amount of available precipitation for strengthening. There is, admittedly, a high degree of uncertainty attached to each

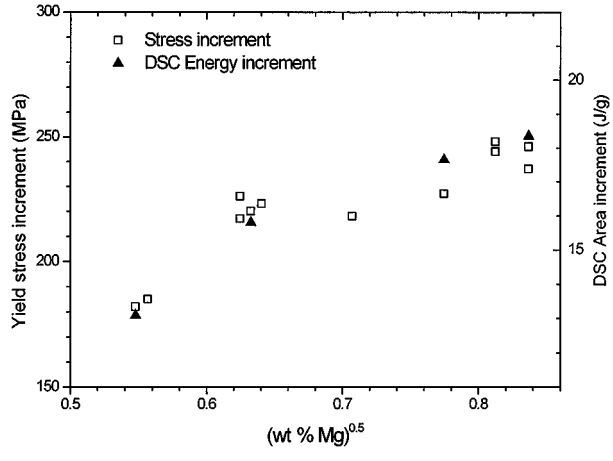

Figure 13 Increments in yield strength and precipitation energy release with increasing bulk Mg concentration. The yield stress increment attributable to Mg was calculated by subtracting a value of 50 MPa for Mg-free Al7%Si [5]. Both vertical axes have a common origin.

step of this comparison process and to the final energy values. However, the general trend seems to be insensitive to the largest uncertainty, which is the energy attributable to Si precipitation.

The transformation temperatures of the β'' peak are relatively insensitive to Mg level, which suggests that the peak ageing conditions will be similarly insensitive to Mg concentration. The subsequent reactions show rather more variation with Mg and the overall trend is that the higher Mg alloys should overage less rapidly than 0.4%Mg. The situation with the 0.3%Mg alloy is too difficult to draw any conclusions from because of the ovelapping of the peaks.

5. Conclusions

The following conclusions may be drawn from this work:

1. Increasing Mg content or cooling rate shifts the liquidus and binary eutectic transformations to a lower temperature.

2. The solidification sequence reported by Bäckerud *et al*. [6] for these alloys is confirmed, but only four of the reactions were detectable by DSC: primary dendrite formation; the binary Al-Si eutectic; ternary Al-Si-Mg_2Si eutectic; and the quaternary Al-Si-Mg_2Si-π AlFeMgSi eutectic. Of these, the ternary reaction was only observed at Mg levels 0.6 wt% and higher, while the other three were observed for all compositions.

3. The latent heat of fusion for Al-7%Si is 447 kJ/kg. This value is independent of Mg content from 0 to 0.7 wt%.

4. The composition of the π-AlFeMgSi intermetallic phase corresponds to a formula of $Al_9FeMg_3Si_5$ in both the as-cast and solution heat-treated states.

5. The Fe-rich phases remaining after T4 solution treatment are mainly π-AlFeMgSi intermetallics in the high Mg alloys (>0.4 wt%); while in the low Mg alloys ($\leq 0.4\%$) they are a mixture of π-phase and β-Al_5FeSi particles.

6. During solution treatment of the low Mg alloys ($\leq 0.4\%$) at 540°C, the π-phase decomposes slowly (over many hours) to release Mg into solution. This decomposition seems to produce very fine Fe-rich precipitates.

7. For solution treatment at 540°C, the optimum Mg content for age-hardening is about 0.5 wt%, above which the excess Mg will remain in π-AlFeMgSi intermetallics which are detrimental to mechanical properties.

8. Neither the dendrite arm spacing nor the presence of Sr-modification seems to have any influence on the precipitation behaviour. The rate of precipitation is relatively insensitive to Mg concentration.

Acknowledgements

The authors would like to acknowledge the support of the Cooperative Research Centre for Cast Metals Manufacturing (CAST), Comalco Aluminum Ltd. in Australia and the Boeing Commercial Airplane Group. We are grateful to Dr. R. Schmidt for the Al-7%Si alloy.

References

1. L. F. MONDOLFO, in "Aluminium Alloys: Structure and Properties" (Butterworths, London, 1976).
2. G. A. EDWARDS, K. STILLER, G. L. DUNLOP and M. COUPER, *Acta Met.* **46** (1998) 3893.
3. D. L. ZHANG, L. H. ZHENG and D. H. STJOHN, *Mat. Sci. and Tech.* **14** (1998) 619.
4. K. T. KASHYAP, S. MURALI, K. S. RAMAN and K. S. S. MURTHY, *ibid.* **9** (1993) 189.
5. C. H. CÁCERES, C. J. DAVIDSON, J. R. GRIFFITHS and Q. G. WANG, *Metallurgical and Materials Transactions A* **30A** (1999) 2611.
6. L. BÄCKERUD, G. CHAI and J. TAMMINEN, "Solidification Characteristics of Aluminium Alloys, Vol. 2" (AFS/SKANAluminium, Des Plaines, IL, USA, 1990) p. 128.
7. D. A. GRANGER, R. R. SAWTELL and M. M. KERSKER, *AFS Transactions* **92** (1984) 579.
8. TAN YEN-HUNG, SHENG-LONG LEE and YU-LOM LIN, *Met. and Mater. Trans A* **26A** (1995) 1195.
9. T. JOENOES and J. E. GRUZLESKI, *Cast Metals* **4** (1991) No. 2, 62.
10. R. I. MACKAY and J. E. GRUZLESKI, *Int J. Cast Metals Res.* **10** (1998) 255.
11. J. A. TAYLOR, D. H. ST JOHN, J. BARRESI and M. J. COUPER, *Materials Science Forum* **331–337** (2000) 277.
12. C. H. CÁCERES, C. J. DAVIDSON and J. R. GRIFFITHS, *Mat. Sci. and Eng.* **A197** (1995) 171.
13. Q. G. WANG and C. H. CÁCERES, *Materials Science Forum* **242** (1996) 159.
14. Q. G. WANG, PhD thesis, The University of Queensland, 1997.
15. C. J. SIMENSEN and T.-L. ROLFSEN, *Z. Metallkd* **88** (1997) 142.
16. S. GOWRI and F. H. SAMUEL, *Metallurgical Transactions A* **23A** (1992) 3369.
17. *Idem., AFS Transactions* **101** (1993) 611.
18. B. CLOSSET and J. E. GRUZLESKI, *ibid.* **90** (1982) 453.
19. S. ARGYROPOULOS, B. CLOSSET, J. E. GRUZLESKI and H. OGER, *ibid.* **91** (1983) 351.
20. P. A. ROMETSCH, L. ARNBERG and D. L. ZHANG, *Int. J. Cast Metals Res.* **12** (1999) 1.
21. J. TAMMINEN, Chemical Communications, No. 2, Univ. of Stockholm, 1988.
22. J. F. HU and E. N. PAN, *Int. J. Cast Metals Res.* **10** (1998) 307.
23. P. N. QUESTED, K. C. MILLS, R. F. BROOKS, B. MONAGHAM, A. T. DINSDALE, A. DAY, M. J. RICHARDSON, R. J. L. ANDON, R. TAYLOR and H. SZELAGOWSKI, in "Modelling of Casting, Welding and Advanced Solidification Processes VII," edited by M. Cross and J. Campbell (TMMMS, 1995) p. 407.
24. G. GUSTAFSSON, T. THORVALDSSON and G. L. DUNLOP, *Metallurgical Transactions A* **17A** (1986) 45.
25. C. GARCIA-CORDOVILLA, E. LOUIS, J. NARCISO and A. PAMIES, *Mater. Sci. and Engg.* **A189** (1994) 219.
26. G. A. EDWARDS, K. STILLER, G. L. DUNLOP and M. J. COUPER, *Materials Science Forum* **217–222** (1996) 713.
27. S. B. KANG, L. ZHEN, H. W. KIM and S. T. LEE, *ibid.* **217–222** (1996) 827.

Received 23 June 1999
and accepted 20 July 2000